JCTC Journal of Chemical Theory and Computation

# Properties and 3D Structure of Liquid Water: A Perspective from a High-Rank Multipolar Electrostatic Potential

Steven Y. Liem and Paul L. A. Popelier*

*School of Chemistry, The University of Manchester, Oxford Road, Manchester M13 9PL, Great Britain, and Manchester Interdisciplinary Biocentre (MIB), 131 Princess Street, Manchester M1 7DN, Great Britain*

Received October 10, 2007

**Abstract:** We propose a new rigid, nonpolarizable high-rank multipolar potential for the simulation of liquid water. The electrostatic interaction is represented by spherical tensor multipole moments on oxygen and hydrogen, up to hexadecupole. The Quantum Chemical Topology (QCT) method yields the atomic multipole moments from a MP2/aug-cc-p-VTZ electron density of a single water molecule in the gas phase. These moments reproduce the experimental molecular dipole and quadrupole moment within less than 1%. Given its high-rank multipole moments, used in conjunction with a consistent high-rank multipolar Ewald summation, the QCT potential is ideal to assess the performance of exhaustive "gas phase" electrostatics in molecular dynamics simulations of liquids. The current article explores the performance of this potential at 17 temperatures between −35 °C (238 K) and 90 °C (363 K) and at 7 pressures between 1 and 10 000 atm. The well-known maximum in the liquid's density at 4 °C is reproduced at 6 °C. Six bulk properties are calculated and found to deviate from experiment in a homogeneous manner, that is, without serious outliers, compared to several other potentials. Spatial distribution functions (i.e., $g_{OO}(r,\Omega)$) and the (more common) radial distribution functions are used to analyze the local water structure. At the lone pair side of a central water, neighboring waters form a continuous horseshoe-like distribution, with substantial narrowing in the central part. The latter feature is unique to the QCT potential. Under high pressure, the local structure undergoes dramatic rearrangement and results in the collapse of second shell neighbors into the interstitial region of the first shell, which is in close agreement with experiment. Our results also corroborate the suggestion that the local hydrogen-bonded network remains largely intact even under such conditions.

## 1. Introduction

Although the properties of liquid water have been the subject of numerous experimental and theoretical studies, this "simple" liquid is still being actively examined. For example, in 2004, Nilsson and co-workers[1] probed the local structure of liquid water by X-ray absorption spectroscopy and X-ray Raman scattering. Perhaps surprisingly their results suggested that most water molecules have only one strong donor and one strong acceptor hydrogen bond. This picture is in stark contrast with the conventional one of locally tetrahedral liquid structure. Shortly after, Nilsson's view was challenged by Saykally and co-workers,[2] who calculated the average number of hydrogen bonds to be 3.3, which is closer to the traditional idea. Nilsson and co-workers then countered this criticism[3] but received an immediate reply[4] from the Saykally group. However, prior to this dispute, both groups could agree[5] on the presence of such single donor and single acceptor species at the surface of liquid water. This was later

* Corresponding author e-mail: pla@manchester.ac.uk.

10.1021/ct700266n CCC: $40.75 
Published on Web 01/12/2008

confirmed by a Car−Parrinello molecular dynamics study[6] on the aqueous liquid−vapor interface.

Experimental investigations into the properties of liquid water at nonambient conditions still constitute an area of active research and so does the design of new potentials.[7] Okhulkov et al.[8] carried out X-ray scattering studies to examine the structure of liquid at pressures of up to $7.7 \times 10^3$ bar. They observed unusual pressure dependence at the shortest intermolecular separation and suggested that under high pressure the second-neighbor shell collapses into the first shell. This explanation was adopted by Eggert et al.[9] in their recent X-ray diffraction study of liquid water under high pressure. In addition, Eggert et al. also observed a rapid increase in coordination number with pressure. This finding is consistent with the results obtained by Schwegler et al.,[10] who used first principles molecular dynamics (MD) simulations to study liquid water under pressure.

Experimental studies are rather limited in their ability to depict a detailed picture of the local structure of liquid water. However, molecular simulation techniques are able to produce comprehensive configurational information. Using the SPC/E water potential, Svishchev and Kusalik[11] carried out MD simulations to characterize the structure of liquid water by spatial distribution functions (SDF), denoted by $g_{AB}(r,\Omega)$ (where $A$ is always $O$ in our analyses while $B$ can be either $O$ or $H$. The symbols $r$ and $\Omega$ refer to radial and angular coordinates, respectively). Spatial distribution functions contain more information than the more familiar radial distribution functions (RDF), which are obtained from the former by orientational averaging. In their study, SDFs established the precise location of the nearest neighbors, lost in the more familiar RDFs. In a subsequent study, Svishchev and Zassetsky[12] used the polarizable point-charge potential (PPC) function to model liquid water. They performed MD simulations of liquid water and calculated the van Hove function in order to examine the dynamic evolution of the structure of water. The 3D molecular density produced by the polarizable point-charge potential model was consistent with their earlier work[11] using the SPC/E model. In addition, they observed that the two H-bond accepting neighbors are less mobile than the H-bond donating neighbors.

Starr et al.[13] examined the structure of supercooled and glassy water under pressure via MD simulations using the SPC/E potential. They found remarkable agreement with neutron-scattering studies for a wide range of temperatures and pressures. Another study at nonambient conditions was carried out by Kalinichev et al.,[14] who used Monte Carlo-(MC) simulations in conjunction with the TIP4P potential and to examine liquid water at pressures up to $10^4$ bar. Using density weighted RDFs, they obtained good qualitative and quantitative agreement between simulation and experiment and demonstrated the persistence of a hydrogen-bonded molecular network in water under high pressures.

Our interest in the structure of liquid water was triggered by a concerted effort to design interaction potentials, initially focusing on the electrostatic component, from a theory called Quantum Chemical Topology (QCT).[15−20] This theory enables an ambiguous partitioning of molecules in atoms, and because of simple atomic additivity, also a partitioning of van der Waals complexes into their constituent molecules. Work in our group focused on expressing the electrostatic interaction between molecules by atomic QCT multipole moments. Considerable attention[21−26] was paid to the convergence of the multipole expansion. Geometries of simple van der Waals complexes[23] and natural DNA base pairs[27] were successfully predicted with a QCT multipolar potential, including hexadecupole moments. The effects of hydrogen-bonding environment on the polarization and electronic properties of water molecules were also studied[28] as well as the asymptotic behavior of the dipole moment of water with increasing water cluster size in liquid water.[29] The first dynamical study, using such a high-rank electrostatic QCT potential, appeared[30] in 2003, examining liquid HF, soon followed by the first such study on pure liquid water[31] at ambient conditions. Throughout this article we refer to the latter paper as Paper I.

So far, the repulsive part of the potential has been covered by the Lennard-Jones potential. Our sustained research effort aiming at extraction of *all* contributions to the interaction potential from reduced density matrices demands to abandon those simple potentials ultimately. This will be subject of a future project outside the scope of this paper. Second, polarization is *not* included in the current potential but we presently work on covering it using machine learning. So far, only one simulation[32] (on the HF dimer) has been carried out with a polarizable QCT potential, in which neural networks predict atomic multipole moments as a function of the positions of the neighboring atoms.

Here the Coulomb part of the atom−atom interaction is represented by electrostatics only, be it accurate at short range, and in conjunction with a fully multipolar Ewald summation. We stress that the current simulation occurred with rigid water molecules and that no attempt was made to introduce "effective" Coulomb interaction. Indeed, we calculated the wave function of a single water molecule, geometry-optimized it in the gas phase, without artificially enhancing the molecular dipole moment or adding polarizability. The purpose of this study is to assess the overall performance of a potential in which the electrostatic part is parameter-free and "taken to the limit". In Paper I the assessment of such a potential took place by comparing a number of bulk properties with experiment and by inspecting RDFs. Here, we add a number of bulk properties, but the emphasis is on the inspection of the orientationally nonaveraged structure of liquid water, now explored over a larger portion of the phase diagram. For this purpose the number of temperatures was more than tripled, and the pressure was investigated up to $10^4$ atm (approximately $10^4$ bar), beyond the previously reported 1 atm.

## 2. Background and Method

**2.1. The QCT Potential.** A single water molecule was geometry optimized at the MP2/aug-cc-pVTZ level[33] using GAUSSIAN98,[34] yielding an OH distance of 0.9614 Å and an HOH angle of 104.067°. The corresponding electron density yields a molecular dipole moment of 1.852 D (debye) (0.7286 a.u.), which deviates by 0.1% from the oft cited and still quoted experimental value of $1.8546 \pm 0.0006$ D (0.7297

± 0.0002 a.u.) determined by Stark measurements.[35] Although possibly fortuitous, this agreement is excellent in view of the wide range generated by respectable levels of theory.[36] For example, a recent CCSD(T) calculation[37] with a 9s6p6d3f/6s4p2d1f basis set yielded a dipole moment of 0.7231 a.u. (or 1.838 D), which curiously deviates more from experiment, now by 0.9%. The molecular quadrupole moment at MP2/aug-cc-pVTZ level is 3.604 DÅ (2.679 a.u.), only different by 0.7% from the experimental value of 3.63 ± 0.04 DÅ (2.70 ± 0.03 a.u.), published[38] by Verhoeven and Dymanus. The CCSD(T) calculation produces 3.532 DÅ (2.626 a.u.), which is still only 2% different to our level of calculation but almost four times more deviating from experiment than the MP2 calculation.

At this stage of our longer term strategy we can justify the rigid body approach because of the success of other rigid body water potentials.[39−41] Furthermore, in a dedicated study[42] on the relative merits of flexible versus rigid models, Tironi et al. highlighted the seriously enhanced computational effort in the presence of high-frequency internal vibrations. They showed that including molecular flexibility and treating it classically does not improve the quality of the models and can even introduce artifacts. This is corroborated by Jorgensen and Tirado-Rives who claim[43] that although flexible models have been explored,[44] classical treatment of the high-frequency vibrations for water is not physically sound. Moreover, Mahoney and Jorgensen stated[44] that the introduction of quantum mechanical effects alleviates some of the problems created by adding classical flexibility to simple water models, reinforcing the idea that real water is more like rigid water models than classical flexible water models.

Using default parameter values, the program MORPHY98[45] computes the multipole moments (up to hexadecapole, rank $\not= 4$) on each atom from the wave function. This is accomplished via a volume integration[46] over each atomic basin $\Omega$. An atomic basin is a portion of 3D space spanned by the collection of gradient paths (trajectories of steepest ascent in the electron density) that are attracted to the nucleus.[15,16,47] The integrand of this volume integration consists of the appropriate spherical tensor ($C(\theta,\varphi)$), weighted by the total charge density $\rho_{tot}(\mathbf{r})$

$$Q_{l0} = \int_\Omega d\mathbf{r}\rho_{tot}(\mathbf{r})r^l C_{l0}(\theta,\varphi)$$

$$Q_{lmc} = \int_\Omega d\mathbf{r}\rho_{tot}(\mathbf{r})r^l C_{lmc}(\theta,\varphi)$$

$$Q_{lms} = \int_\Omega d\mathbf{r}\rho_{tot}(\mathbf{r})r^l C_{lms}(\theta,\varphi) \quad (1)$$

where $\rho_{tot}(\mathbf{r}) = \sum_\mathbf{A} Z_\mathbf{A}\delta(\mathbf{r} - \mathbf{R_A}) - \rho(\mathbf{r})$, $Z_A$ is the charge of nucleus $A$ located at position $\mathbf{R_A}$, and the functions $C_{lmc}(\theta,\varphi)$ and $C_{lms}(\theta,\varphi)$ are real normalized spherical harmonics of rank $l$. Other than the atomic charge $Q_{00}$, there are three dipole moments ($l=1$), denoted by $Q_{10}$, $Q_{11c}$, and $Q_{11s}$, which correspond to the Cartesian components $\mu_z$, $\mu_x$, and $\mu_y$, respectively. Instead of the redundant six Cartesian quadrupole moments there are only five spherical-tensor quadrupole moments ($l=2$), denoted $Q_{20}$, $Q_{21c}$, $Q_{21s}$, $Q_{22c}$, and $Q_{22s}$. There are seven octopole moments ($l=3$) and nine hexadecapole moments ($l=4$). The values for all moments are listed in Table S1 as Supporting Information. We note that our potential shares its multipolar character with Stone's ASP-W2 potential.[48]

The total potential energy ($E_{pot}$) between any two water molecules has two contributions

$$E_{pot} = E_{elec} + 4\epsilon\left[\left(\frac{\sigma}{r_{OO}}\right)^{12} - \left(\frac{\sigma}{r_{OO}}\right)^{6}\right] \quad (2)$$

where $E_{elec}$ corresponds to the electrostatic interaction energy between two water molecules, and $r_{OO}$ is the distance between the two oxygen nuclei. The other contribution is the Lennard-Jones term, containing $\epsilon$ and $\sigma$, which are the familiar well depth and collision diameter. These are the only two parameters in $E_{pot}$, and they were fitted to both the density of liquid water and the shape of experimental RDFs at 298 K and 1 atm. The collision diameter turned out to be 3.140 Å and the well depth 0.753 kJ/mol. The two geometric parameters describing the (symmetric) rigid water molecule were fixed at the values mentioned above. The values of the two geometric and two Lennard-Jones parameters are the same as in paper I.

The $E_{elec}$ term can be evaluated from eq 3

$$E_{elec} = \frac{1}{2}\sum_A \sum_{B\neq A} E_{elec}(A,B) \quad (3)$$

where $A$ and $B$ are oxygen or hydrogen atoms, each belonging to different water molecules. In a previous publication[23] we explicitly showed that eq 3 can be re-expressed in terms of a multipole expansion as follows

$$E_{elec}(A,B) = \sum_{l_A l_B m_A m_B} T_{l_A l_B m_A m_B} Q_{l_A m_A}(\Omega_A) Q_{l_B m_B}(\Omega_B) \quad (4)$$

where $T_{l_A m_A l_B m_B}$ is a purely geometric interaction tensor, only depending on the relative orientation of the local frames centered on each nucleus and their internuclear distance, and $Q_{lm}$ are the $2l+1$ multipole moments of rank $\lambda$ with respect to the local frames. The (expansion) rank $L = l_A + l_B + 1$ is typically used to monitor the convergence of an atom−atom electrostatic interaction energy. In Paper I it was shown that $L$ needs to be at least equal to 5 to observe liquidlike behavior, based on oxygen−oxygen pair distribution functions $g_{OO}(r)$. If DLMULTI were (substantially) modified to handle $L$ values larger than 6, which is a major project, then bulk properties could be more completely monitored for convergence. However, we have implemented an open-ended electrostatic interaction code that enables the evaluation of eq 4 for arbitrary rank $L$. We showed before[49] that the atom−atom interaction energy profile versus $L$ of a typical O and H in the hydrogen bond between two water molecules in the water dimer had definitely converged at $L = 5$.

**2.2. Simulation Details.** As with our previous water simulation, the MD simulation was carried out by the DLMULTI program, which is a modified version of the DLPOLY code.[50,51] A major feature of DLMULTI is the derivation and implementation (by Dr. M. Leslie formerly at Daresbury Labs) of an Ewald summation, generalized beyond point charges, to high rank multipole moments. This Ewald summation is completely consistent with the spherical

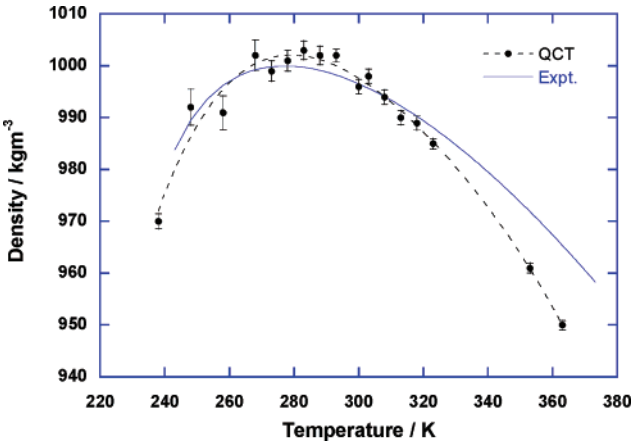


***Figure 1.*** Density of simulated water at 1 atm compared to experimental value.

tensor formalism, which is the basis of the interaction within the simulation box. DLMULTI calculates the long-range contribution of all multipole−multipole interactions using this Ewald summation. A cubic primary cell with full periodic boundary conditions, containing $216 = 6^3$ water molecules, was used for all simulations. Paper I showed that this size is large enough to achieve insignificant system size dependence. We imposed a cutoff distance of $2.5\sigma$ for the Lennard-Jones interaction between oxygen atoms. The time-step size used to integrate the equations of motion was 0.5 fs. The results presented in this article are averaged from run lengths of at least 300 ps after an equilibration period of 20−50 ps.

**2.3. Analysis of Bulk Properties.** In Paper I we already defined and discussed the isobaric heat capacity ($C_p$), the thermal expansion coefficient ($\alpha$), the self-diffusion coefficient ($D$), and the temperature of maximum density. In this study, we evaluated three additional properties of liquid water, namely the constant temperature heat capacity ($C_v$), the isothermal compressibility ($\kappa_T$), and the shear viscosity ($\eta$). The constant temperature heat capacity can be calculated from eq 5

$$C_v = \left(\frac{\partial E}{\partial T}\right)_P \tag{5}$$

where *E, p, and T* are the total energy, temperature, and pressure of the system, respectively. The isothermal compressibility $\kappa_T$ can be evaluated from eq 6

$$\kappa_T = -\frac{1}{V}\left(\frac{\partial V}{\partial p}\right)_T \tag{6}$$

where $V$ is the volume of the system. The shear viscosity was evaluated from a NVT simulation using the Einstein relation, eq 7,

$$\eta = \frac{1}{2}\frac{V}{k_B T}\lim_{t\to\infty}\frac{d}{dt}\langle \Delta P_{\alpha\beta}{}^2(t)\rangle \tag{7}$$

where $\alpha\beta = xy,xz,yz$ and $\Delta P_{\alpha\beta}(t)$ is the "displacement" of $P_{\alpha\beta}(t)$, which is given by eq 8

$$\Delta P_{\alpha\beta}(t) = \int_0^t P_{\alpha\beta}(t')dt' \tag{8}$$

where $P_{\alpha\beta}(t)$ is the off-diagonal elements of the pressure tensor.[52]

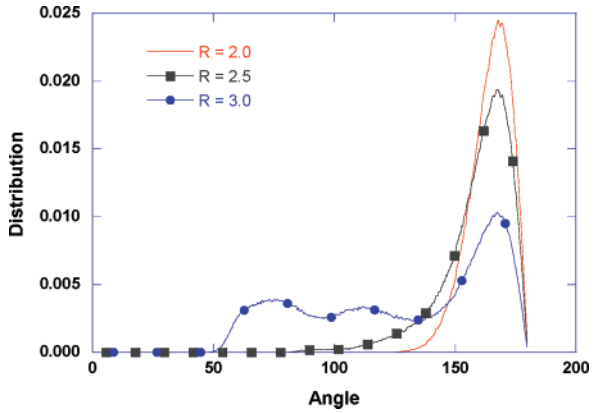


***Figure 2.*** Comparison of the distribution of O−H...O angles at 300 K using different cutoff values for the O...H distances (in Å).

***Table 1.*** Calculated and Experimental Properties of Liquid Water at 300 K (27 °C) and 1 atm

| property | QCT | expt | %Δ[e] |
|---|---|---|---|
| temperature of maximum density (°C) | 6. | 4.[a] | - |
| $D/\times 10^9$ m$^2$ s$^{-1}$ | 1.44 | 2.30[b] | −37 |
| $\alpha/\times 10^5$ K$^{-1}$ | 28 | 27.6[a] | 1 |
| $\kappa_T/\times 10^6$ atm$^{-1}$ | 38 | 45.6[a] | −17 |
| $C_p$/J K$^{-1}$ mol$^{-1}$ | 82 | 75.3[c] | 9 |
| $C_v$/J K$^{-1}$ mol$^{-1}$ | 106 | 74.4[c] | 42 |
| density/kg m$^{-3}$ | 996.0 | 996.5[a] | - |
| $\eta$/cp | 1.2 | 0.85[c] | 41 |
| enthalpy/kJ mol$^{-1}$ | −42.7 | −41.5[d] | −3 |

[a] Reference 58. [b] Reference 72. [c] Reference 73. [d] Reference 74. [e] Percentage deviation from experiment defined as $100(x_{comp}-x_{exp})/x_{exp}$ where $x$ is an experimental or computed property.

**2.4. Analysis of Local Structure.** The short-range structure in liquid water has been examined by various analysis techniques. These include the RDF $g(r)$, the coordination number $n(r)$, intermolecular structural properties (e.g., angles, distances), and three-dimensional SDFs. The latter tool was employed by Svishchev and Kusalik[11] to examine the structure of water using the SPC/E potential. It is a measure of the distribution of neighboring molecules (or a specific type of atoms) around a central molecule. SDFs give a detailed description of the immediate environment adjacent to a molecule by utilizing distribution functions that span both the radial and angular coordinates of the separation vector between species of interest.

Here we describe the procedure of evaluating the SDF of oxygen−oxygen, $g_{OO}(r,\Omega)$. The term *system* refers to the simulation box (which contains 216 molecules). Each molecule in the system is designated as the "central molecule", one at a time. Since we are interested in the immediate environment of the central molecule, we impose a distance-based selection criterion in order to identify the neighbors. The cutoff distance for the O...O separation was chosen to be 3.5 Å, which is the location of the first minimum in $g_{OO}(r)$. For an arbitrary configuration ("snapshot") of the system, the neighbors of the central molecule are examined. This examination warrants a common reference orientation for each central molecule and its environment. This is achieved by translating and rotating the system

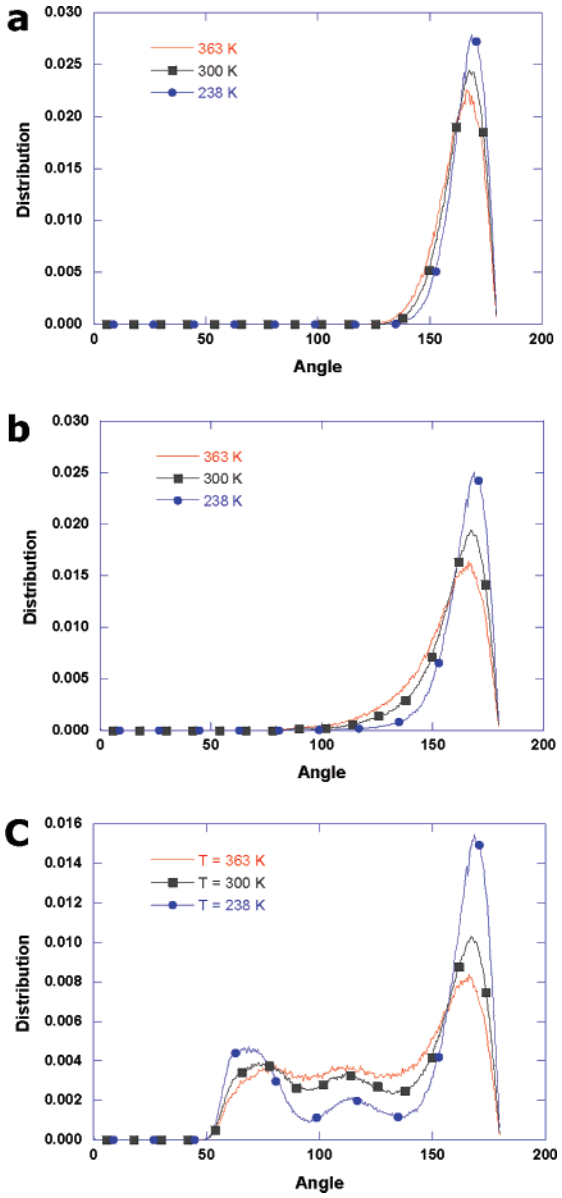


***Figure 3.*** Comparison of the distribution of O−H...O angles at different temperatures. The cutoff distances are (a) 2.0 Å, (b) 2.5 Å, and (c) 3.0 Å.

such that the oxygen atom of the selected central molecule lies at the origin of the system, one O−H bond coincides with the X-axis, and the other O−H bond lies in the XY plane. As a result, all neighboring molecules are viewed from the same perspective. Subsequently, the spherical volume (with radius 5.5 Å) is partitioned into small "grid elements", by installing a 3D grid centered at the central oxygen. Typically there are 110 × 110 × 110 such grid elements. Then a frequency counter determines the number of oxygens (belonging to neighboring molecules) that are located within each grid element. When all molecules in the system are examined, each being a central molecule in turn, the frequency of oxygen atoms appearing in each grid element, $n_O$, is known. In order to obtain a distribution of oxygens around a *single* central molecule, this frequency needs to be normalized by the number of oxygen atoms in the system, $N_O$. The value $n_O/N_O$ then gives the desired mean frequency of neighboring oxygens located around the oxygen of a *single* central molecule. This process can be repeated for all configurations generated from a MD run. However, it is more sensible to use a portion of these configurations (e.g., every 500$^{th}$ configuration). The value $n_O$ is then incremented over all selected configurations. In order to correct for this accumulation, $n_O$ must be divided by the number of configurations included in the evaluation, $N_c$, resulting in $n_O/[N_O N_c]$.

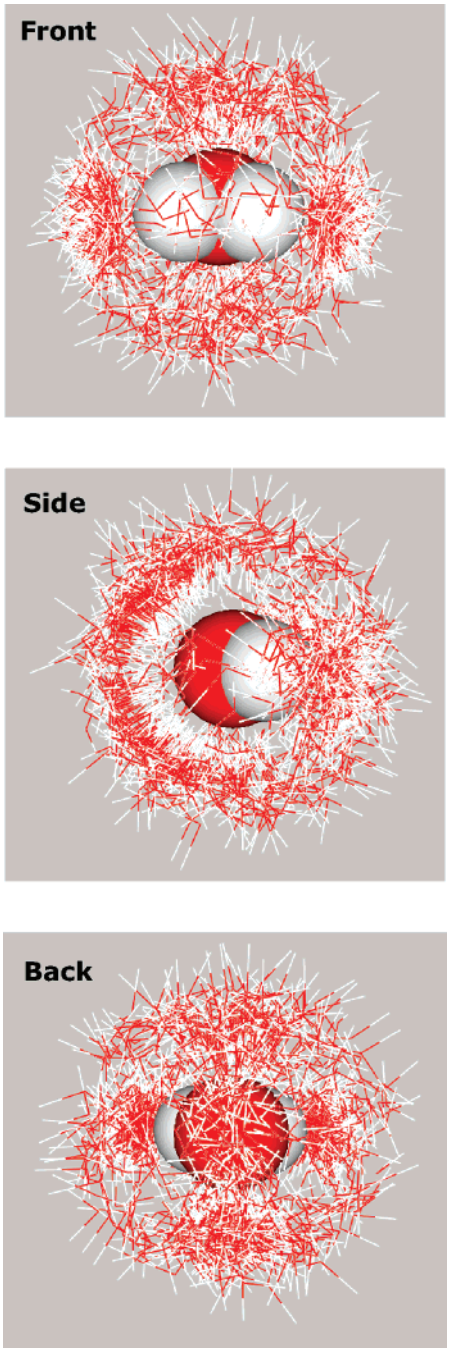


***Figure 4.*** Location of neighboring molecules adjacent to each molecule in the system. Three different views are presented: front, side, and back view.

Finally, the average number of oxygen atoms appearing in each grid element is given by $[N_O V_{elem}]/V_{syst}$ where $V_{elem}$ is the volume of the grid element (assuming a homogeneous distribution of oxygen atoms in the system), and $V_{syst}$ is the volume of the system. We used this factor to normalize the

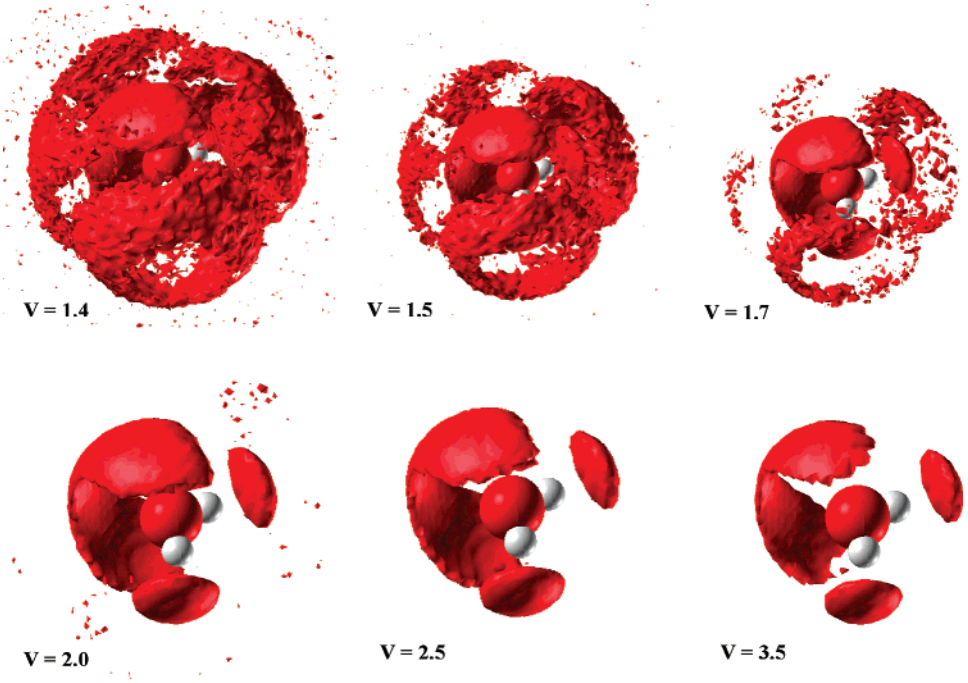


***Figure 5.*** Six different isovalues of the SDF illustrating the variation in the immediate environment of a central water molecule (plotting scales adjusted visually).

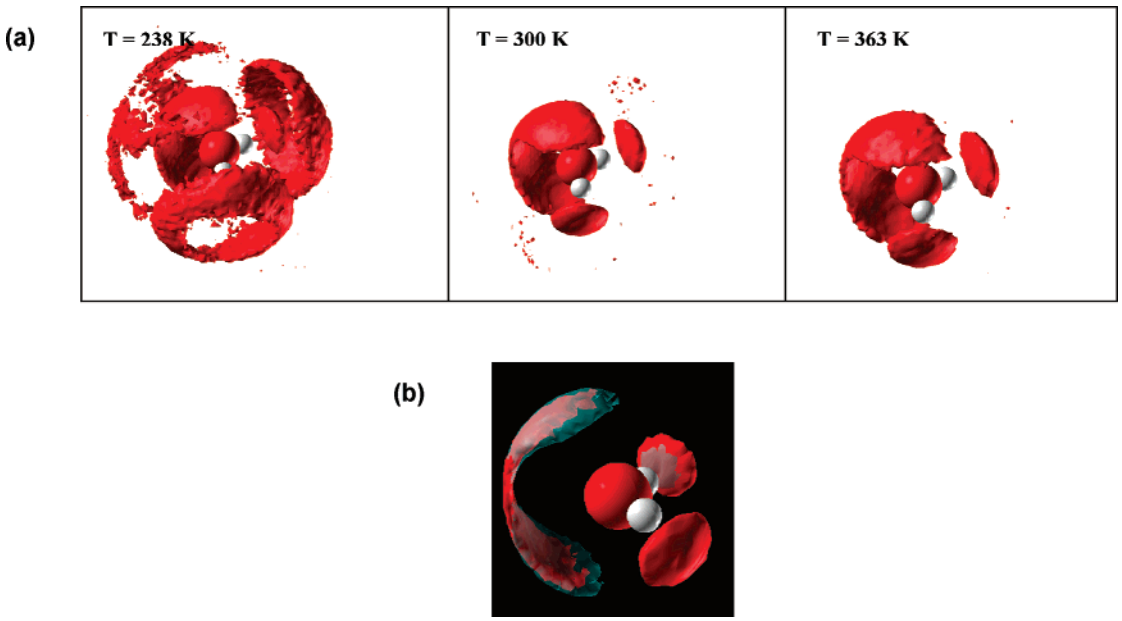


***Figure 6.*** (a) SDF isosurfaces with a value of 2.0 illustrating the variation of the immediate environment of a central water molecule at different temperatures (plotting scales adjusted visually). (b) Comparison of spatial distribution functions of oxygen atoms (showing the first shell neighbors only) $g_{OO}(r,\Omega)=2$, at two different temperatures, 238 K (−35 °C) (cyan) and 363 K (90 °C) (red) (at 1 atm).

mean value, $n_O/[N_O N_c]$, to give a value that is relative to the mean oxygen density of the system. The final quantity, $g_{OO}(r,\Omega)$, is then defined in eq 9. If the grid element size is sufficiently small, then the density function $g_{OO}(r,\Omega)$ appears continuous and meaningful constant-density envelopes can be plotted, as shown in Figures 5, 6, and 9.

$$g_{OO}(r,\Omega) = \frac{n_O}{N_O N_C}\left[\frac{N_O V_{elem}}{V_{syst}}\right]^{-1} \qquad (9)$$

The corresponding formula for $g_{OH}(r,\Omega)$ can be easily obtained by replacing $n_O$ by $n_H$ in eq 9, where $n_H$ is the frequency of hydrogen atoms appearing in each grid element. Second, $N_O$ must be replaced by $N_H$, the number of hydrogen atoms in the system.

## 3. Results and Discussions

Compared to the NPT simulations of liquid water at ambient pressure in Paper I we extended the temperature range from

***Table 2.*** Averaged System Density and Calculated Diffusion Coefficient at 300 K at Various Applied Pressures

| pressure/atm | density/kgm$^{-3}$ | $D/\times 10^9$ m$^2$ s$^{-1}$ |
|---|---|---|
| 1 | 996 | 1.44 |
| 1000 | 1045 | 1.53 |
| 2000 | 1086 | 1.42 |
| 4000 | 1149 | 1.11 |
| 6000 | 1200 | 0.88 |
| 8000 | 1242 | 0.70 |
| 10000 | 1274 | 0.58 |

238 K to 363 K (−35 °C to 90 °C) with runs at 17 different temperatures. We also conducted several NVT simulations in order to calculate the constant volume heat capacity. Finally, we performed NPT simulations at nonambient pressures (between 1 and 10 000 atm at 300 K, 7 pressures in total) in an attempt to understand the effect of pressure on the structure of liquid water.

**3.1. Simulations at Ambient Pressure.** *3.1.1. Bulk Properties.* The various properties evaluated from the ambient pressure simulations (1 atm, 300 K) are summarized in Table 1. The variation of the density of the system as a function of temperature is shown in Figure 1 (numerical values in Table S1). The graph clearly shows the existence of a temperature of maximum density at around 280 K. By numerically differentiating a fitted fourth order polynomial, the maximum is determined to be 279 K (6 °C). This maximum is not affected by the presence of the error bars. This value deviates by only 2 °C from the well-known experimental value of 277 K (4 °C). The availability of simulation runs at 12 extra temperatures, compared to the 5 runs of Paper I, improved the quality of the prediction. Indeed, in Paper I the rather slowly converging property of maximum density temperature was overestimated by about 10 °C. When comparing the overall shape of the experimental and simulated density-versus-T curves in this work, the density of the simulated water decreases at a faster rate at both ends of the temperature range (i.e., the curvature of the simulated curve is larger). However, Monte Carlo simulations (at 1 atm) carried out[53] for the SPC and TIP3P models showed no maximum at all within the [−50 °C, 100 °C] interval. The TIP4P model put the maximum at −15 °C (258 K), SPC/E at −38 °C (235 K).[54] In contrast, the TIP5P model, which was specifically designed to correctly predict the temperature of maximum density, does indeed reproduce the correct value of 4 °C at 1 atm.

The self-diffusion coefficient $D$ deviates slightly more from the experimental value compared to Paper I, where $D = 1.5 \times 10^{-9}$ m$^2$ s$^{-1}$ was reported. Nevertheless, the current 37% deviation from experiment is still respectable compared to other potentials, which yield values varying from 1.9 (TIP4P-FQ) to 5.2 (TIP3P). Popular point charge models such as TIP3P, TIP4P ($D = 3.3 \times 10^{-9}$ m$^2$ s$^{-1}$) and SPC ($D = 3.9 \times 10^{-9}$ m$^2$ s$^{-1}$) all substantially overestimate $D$. The TIP5P model predicts D to be $2.6 \times 10^{-9}$ m$^2$ s$^{-1}$, which is only 12% off, and SPC/E scores well with $D = 2.5 \times 10^{-9}$ m$^2$ s$^{-1}$. Chaplin provides a continuously updated Web site[55] comparing a large number of potentials in terms of their performance in predicting bulk properties. In 2002, Guillot[44] compared the self-diffusion coefficient of 32 water potentials and found that about 40% overestimated its value, about 40% underestimated it, whereas about 20% predicted it correctly. The addition of quantum effects[43,56,57] is known to increase the value of $D$ substantially. Thus it is promising that the QCT model underestimates $D$, in the absence of quantum effects.

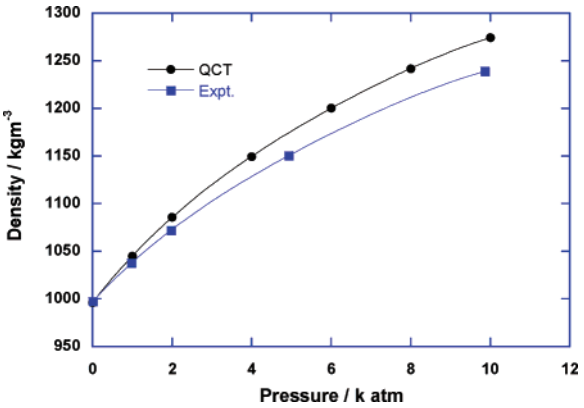


***Figure 7.*** Density of simulated water at different pressures compared to experimental value.

The thermal expansion coefficient, α, has considerably improved compared to Paper I, where it was reported as $35 \times 10^{-5}$ K$^{-1}$. Now referring to an experimental[58] value, evaluated exactly at 300 K (27 °C), the current re-evaluation of α coincides with the experimental value. Other well-known potentials and their recent modifications always overestimate α, sometimes by more than 200%. For example, at 25 °C, TIP3P, TIP4P, and TIP5P predict[59] it to be 92, 44, and 63, respectively. In the SPC series, SPC, SPC/E, SPC/A, SPC/L,[41] COS/B2, COS/G2, and COS/G3[60] predict α to be 73, 56, 80, 75, 97, 57, and 70, respectively, at 300 K (27 °C).

The isothermal compressibility, $\kappa_T$, predicted by QCT to be $38 \times 10^{-6}$ atm$^{-1}$, turns out to underestimate experiment by 17%. From the TIPnP series of potentials, only the TIP5P value of $41 \times 10^{-6}$ atm$^{-1}$ comes closer to experiment than the QCT potential, the other TIP potentials overestimating experiment by at least 40%. The SPC series mentioned above predicts values from 39.5 to $51.7 \times 10^{-6}$ atm$^{-1}$ and hence scores better than QCT. It is conceivable that a $\kappa_T$ value computed from QCT simulations at more than 7 different pressures may lead to better agreement with experiment.

The heat capacity at constant pressure, $C_p$, is a property that clearly benefited from the extra simulation runs at 12 new temperatures. Once predicted to be 105 J mol$^{-1}$ K$^{-1}$ in Paper I, it is now 82 J mol$^{-1}$ K$^{-1}$, overestimating experiment by only 9%. Whereas TIP5P predicted the best $\kappa_T$ value (out of the TIPnP series), it now predicts the worse $C_p$ value, that is, 122 J mol$^{-1}$ K$^{-1}$, which deviates from experiment by 62%. The SPC model is able to match experiment virtually perfectly, but its recent modifications (mentioned above) overestimate experiment with a value as high as 94.1 J mol$^{-1}$ K$^{-1}$.

The heat capacity at constant volume, $C_v$, again suffers from the more modest number of pressures at which simulations were conducted. As a result, the QCT prediction

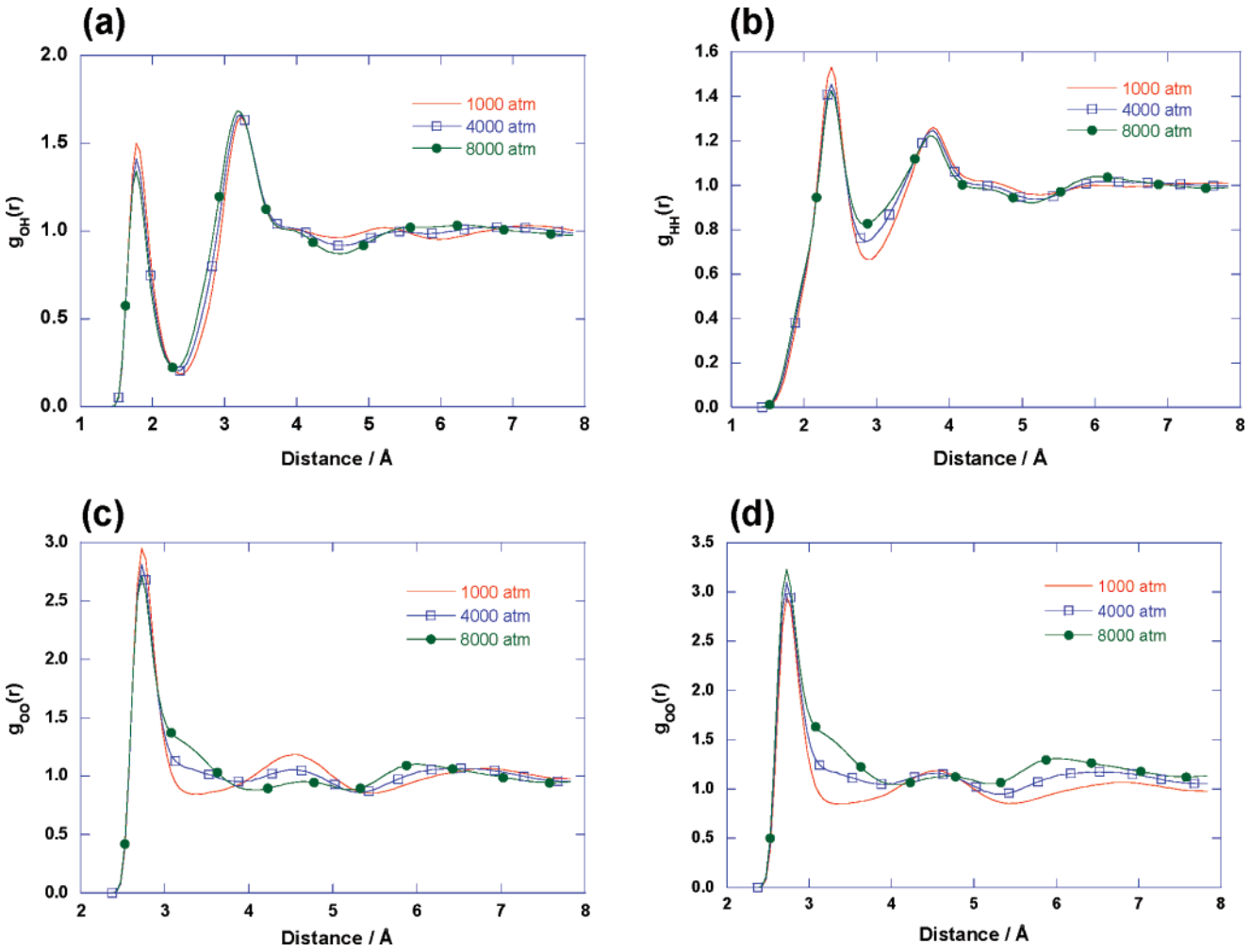


***Figure 8.*** Comparison of RDFs at three different pressures. (a) OH, (b) HH, (c) OO, and (d) density-weighted ("normalized") OO.

of 106 J mol$^{-1}$ K$^{-1}$, is expected to deviate substantially from experiment. Indeed, it does so by 42%. The papers we consulted for the results of familiar potentials, as discussed above, do not report $C_v$.

The QCT potential predicts shear viscosity ($\eta$) only moderately well, overshooting experiment by 41%. However, the SPC model performs equally poor, undershooting experiment by 42%. Only SPC/E does substantially better, predicting a value of 0.91 cp, which is only 7% off the experimental value of 0.85 cp. The TIP5P model predicts 1.49 cp, which is 75% off.

*3.1.2. Structure.* The local structure of the liquid water was examined by monitoring the distribution of O−H...O angles and the SDFs. The distribution of the O−H...O angle was computed by calculating the angle formed by an H atom from a neighboring molecule with the O−H bond from a given central molecule. We selected neighboring molecules by setting the cutoff values for the O...H distance to 2.0, 2.5, and 3.0 Å. Figure 2 illustrates the variation in the distribution of the O−H...O angle for these three cutoff distances. For 2.0 Å, the distribution is a single well-defined peak centered at approximately 169°. The peak is slightly skewed to the left and tails off rapidly for values smaller than 150°. At the cutoff of 2.0 Å, most water pairs can be regarded as hydrogen bonded to each other. The distribution at the 2.5 Å cutoff is similar, but the tailing off (at the left of the maximum) is slower. This follows from the fact that the maxima of the two peaks, 2.5 Å and 2.0 Å, practically coincide but the angle at which the distribution vanishes is 86° and 127°, respectively. The distribution for the largest cutoff of 3.0 Å is qualitatively different from the two others. Now there are smaller peaks left of the main one, at angles well below 150°, one centered at 113° and the other at 74°.

The effect of temperature (238, 300, and 363 K) on the O−H...O angle distribution is shown in Figure 3. As expected, the height of the peak near 170° decreases with increasing temperature for all three O...H distance cutoff values. Also, the peaks broaden, while the tail ends located between 50 and 150° become less well defined. The impact of temperature rise is significantly smaller for shorter cutoffs.

A direct way to analyze the local structure of liquid water is visualizing a snapshot of the simulated system. Figure 4 shows the location of neighboring molecules adjacent to each molecule in the system. This picture is generated by selecting all neighboring molecules with a O...O distance of less than 3.5 Å from the central molecule. Note that each selected "central molecule" was rotated and translated (together with the neighbors) to coincide with the position of the large

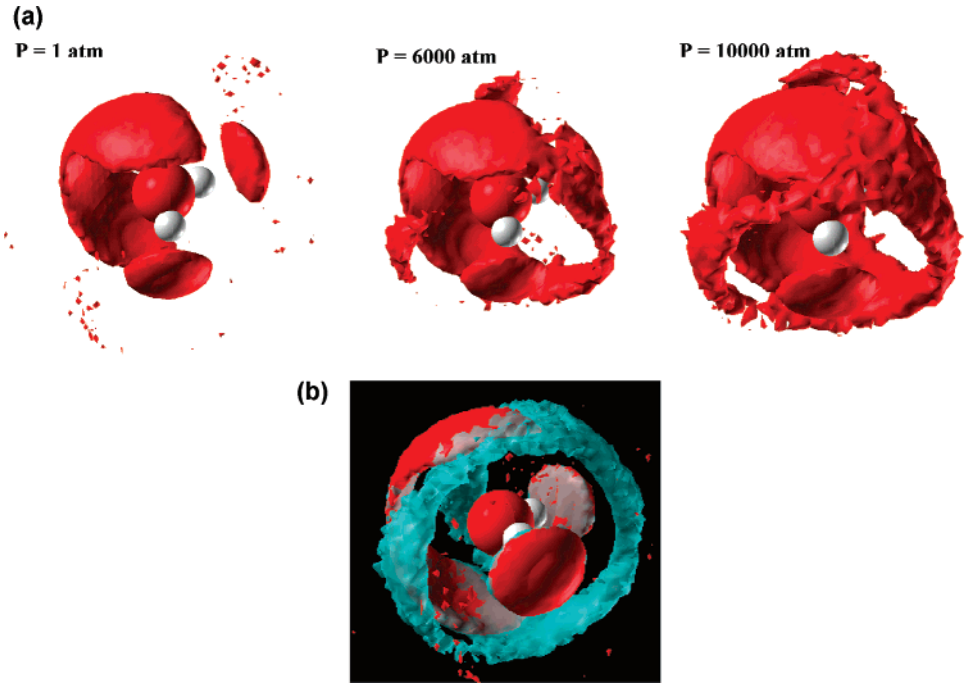


***Figure 9.*** (a) SDF isosurfaces with a value of 2.0 ($g_{OO}(r,\Omega)=2$) illustrating the variation of the local environment of a central water molecule at three different pressures (plotting scales adjusted visually). (b) Comparison of spatial distribution functions of oxygen atoms (showing the 1st shell neighbors only) at two different pressures, 10 000 atm (cyan) and 1 atm (red) (at 300 K).

molecule in the center of Figure 4a−c. Neighbors are concentrated in three regions of space around the central water molecule. Two regions are adjacent to hydrogen atoms of the central water. These regions consist of molecules acting as hydrogen bond acceptors to the central water molecule. The third region encircles the lone pair zone of the central oxygen in the shape of a horseshoe. The "side view" of Figure 4 gives the clearest image of this region, which consists of donor molecules forming hydrogen bonds with the central oxygen atom. This continuous distribution is in agreement with Finney's observation[61] that the negative charge around the oxygen atom should be regarded as a single (contiguous) zone rather than as two distinguished lobes.

In contrast with many familiar water potentials, the width of the "horseshoe" narrows gradually but significantly toward the middle part, in the plane of the central water molecule (see "back view"). To the best of our knowledge, this feature has not been observed in other water (traditional) potentials. Alternative potentials, such as PPC,[12,62] SPC/E,[11] and TIP4P,[63] typically show a *widening* in the middle region. We believe that this is a direct consequence of the multipole nature of our potential, whose improved directionality results in accurate geometry prediction of small water clusters.[64] Consequently, we believe this is a genuine structural property for liquid water. It should be noted that in the space between these three regions, the existence of water molecules is significantly less likely but not negligible.

An alternative way of examining the local structure is to use the SDFs where the distribution and number of adjacent molecules (in our case oxygen atoms actually) are represented by isosurfaces of specific values. A higher isovalue means a higher oxygen and hence water concentration. Figure 5 shows the distribution at six different isovalues, i.e., 1.4, 1.5, 1.7, 2.0, 2.5, and 3.5. For isovalues above 2.0, the information deduced from the isosurfaces is essentially identical to that in Figure 4, apart from the fact that the three regions are more readily identifiable. For lower values, molecules further away from the central molecule start to appear, corresponding to the second shell of oxygen atoms. This secondary structure becomes more notable at the 1.4 and 1.5 isovalues. Two separate circular rings appear, each centered on a "flattened sphere" (consisting of acceptor oxygens) next to each of the hydrogen atoms of the central water. The secondary structure adjacent to the "horseshoe" shaped region appears as a pair of "wings".

Let us focus on the relationship between oxygens in a circular ring and oxygens in the flattened sphere beneath it. In particular, we ask if such pairs of oxygen atoms are hydrogen-bonded. A natural criterion to decide on this question is knowledge of the average O...O distance. We know from the $g_{OO}(r)$ curves (Figure S2 in the Supporting Information and also Figure 8c) that hydrogen-bonded oxygens are separated by approximately 2.7 Å and definitely less than 3 Å. Figure 4 enables the measurement of O...O distances, and via the straightforward correspondence between Figures 4 and 5 we can infer distances in Figure 5. Distances between the appropriate oxygen pairs were sampled directly in the snapshots appearing in Figure 4. The spread in a typical sample of distances turned out to be very small. We concluded that the average O...O distance is about 2.9 Å. Hence, this supports the existence of a network of hydrogen bonds between the first and second shell.

The effects of temperature on the local structure of liquid water are illustrated in Figure 6 by means of SDF=2.0 isosurfaces. The distribution of oxygen atoms is slightly more

dispersed (i.e., the volume enclosed by the isosurface is bigger) at 363 K when compared with 300 K. Perhaps more surprisingly is the appearance of the secondary structure at 238 K at the high isovalue of 2.0. This shows that the local tetrahedral network is enhanced by the reduction in temperature.

**3.2. Simulations at High Pressure.** The results of the nonambient pressure simulations are summarized in Table 2, and the variation of liquid density as a function of pressure is compared with experimental results in Figure 7. The comparison shows that the simulated water mimics its real counterpart reasonably well with larger deviations at higher pressures. Furthermore there is tentative evidence in Table 2 for the reported[65−68] maximum in diffusion coefficient at elevated pressures, which is one of the well-known anomalies of liquid water.

RDFs are a useful tool to monitor the local structure of a liquid and can be readily obtained by experiment or computer simulations. Figure 8 shows the results of various RDFs derived from the simulations. The effect of pressure on the HH and OH RDFs (in Figure 8a,b) is gradual and small. There is no significant change in the overall form but with only limited decrease in the peak heights and decrease in well depth of the first broad minimum. In contrast, Figure 8c shows that the OO RDF changes substantially with pressure. The second peak at around 4.5 Å gradually disappears (i.e., flattens), while a shoulder starts to develop on the right-hand side of the first peak (at around 3.2 Å) as the pressure is increased. However, a simple comparison of the current RDFs may not be appropriate because the pressure increase causes a considerable change in density. This is why we corrected the OO RDF for this change in density, as shown in Figure 8d. The density-weighted or normalized RDF curves show a different picture. The height of the first peak increases with pressure rather than decreases. More importantly, the disappearance of the second peak (for 1000 atm) is not due to reduction in its peak height. Rather, it can be attributed to the notable increase in the RDF in regions between 3 and 4 Å and between 5 and 7 Å. This bears remarkable resemblance to the molecular distribution functions obtained from X-ray diffraction of liquid water at pressures up to 7700 bar by Okhulkov et al.[8]

Our results also indicate that the coordination number rises from 5 to about 7.5 when the pressure is increased from 1 to 10 000 atm. This is consistent with the findings of Eggert et al.[9] and a recent first principles MD simulation of liquid water[10] where the coordination number also increases with pressure. Even at 1 atm, previous studies have indicated that the coordination number is greater than four.[11,69]

A more direct way of examining the effect of pressure on local structure is provided by SDFs, as shown in Figure 9). It can be seen that high pressure has a dramatic effect on the short-range structure. A considerable number of oxygens start to appear in regions where they were rare at ambient pressure. At 10 000 atm, the "horseshoe" region has notably morphed into a complete ring occupying space in between the two hydrogens of the central water. In addition, the isosurface with lower values (e.g., 1.5) shows similar features. However, the secondary ring structure that appeared

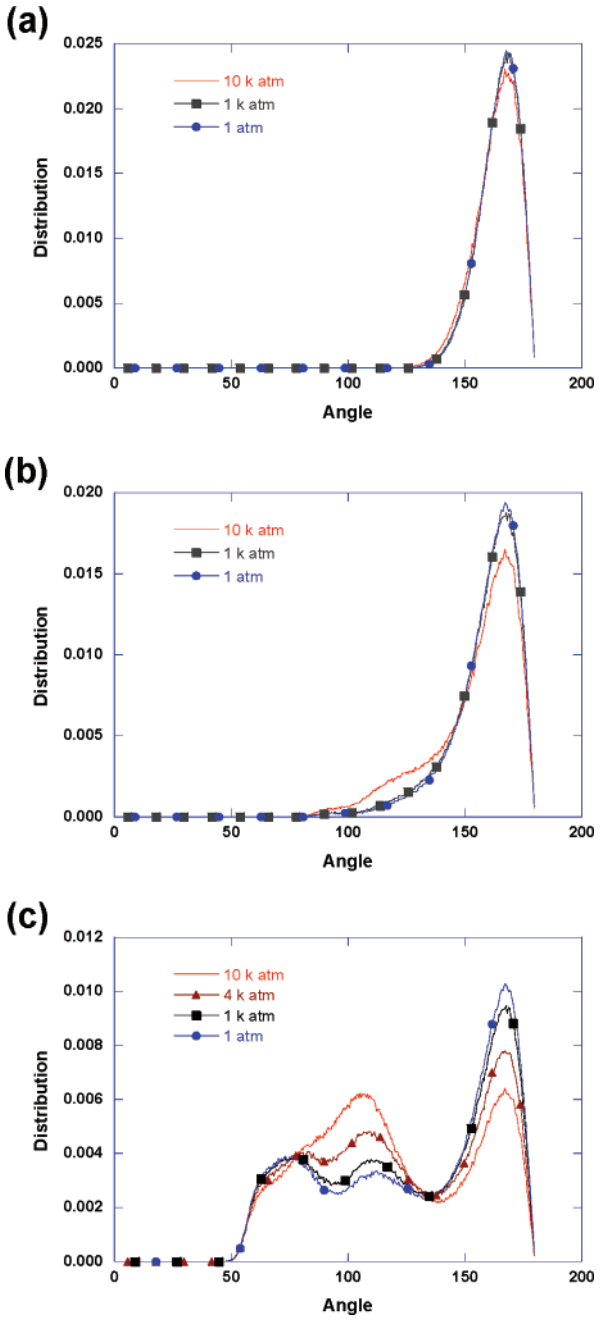


***Figure 10.*** Comparison of the distribution of O−H...O angles at three different pressures. The cutoff distances are (a) 2.0 Å, (b) 2.5 Å, and (c) 3.0 Å.

at ambient pressure is now much less significant indicating a decrease in the amount of water associated with it. Moreover, the secondary "wing"-like structure (see $T = 238$ K in Figure 6) is completely absent at this elevated pressure (10 000 atm). This is a unique piece of evidence that confirms the collapse of second-neighbor shell molecules into the first shell, which is inferred from X-ray diffraction[9] and X-ray scattering experiments.[8] These additional molecules also contribute to the OO RDF, and they are responsible for the increase in $g(r)$ between 3 and 4 Å.

The O−H...O angle distributions (see Figure 10) can also shed some light onto the change induced by the applied pressure. As in the ambient pressure case, the change in

distribution for close neighbors (cutoff = 2.0 Å) is minimal even at the highest pressure. However, the impact of increased pressure on the distribution for neighboring molecules of up to 3.0 Å is quite remarkable. There is a substantial reduction in height of the peak at 170° in conjunction with an extensive change in the tail of the distribution (50−140°). Upon pressure increase, the two smaller peaks merge to form one peak centered at 110° and the number of molecules belonging to this range increases dramatically. Again, this is consistent with what one observes in the RDFs and SDFs. This increased angular distortion in the O−H...O angle distribution has also been suggested by Khan et al.[70]

It has been suggested[71] that the hydrogen-bonded molecular network remains almost intact even at extreme high pressures. This is supported by the finding of Kalinichev et al.[14] who used MC simulations in conjunction with the TIP4P water potential to show that the number of hydrogen-bonded neighbors does not change significantly even in such severe conditions. Our SDF results corroborate this result because the regions occupied by the first shell neighbors at 1 atm and 10 000 atm remain invariant (see Figure 9). However, it should be noted that there is a significant difference in the distribution of the nearest neighbors between our QCT potential and the TIP4P one.[63]

The stability of the hydrogen-bonded molecular network can also be seen in the O−H...O angle distributions because they remain essentially the same for a cutoff up to 2.5 Å, even at the highest pressure. In addition, we believe that the appearance of molecules in the interstitial regions (see Figure 9) is the cause for suggested change in the O...O...O and O−H...O angle distributions as proposed by Urquidi et al.[71] and Khan et al.[70]

## 4. Conclusions

We carried out extensive simulations of liquid water using a QCT potential. In view of its high-rank multipolar character the description of the electrostatic interaction at short range is expected to be accurate, except for the lack of polarization. We have explored a part of the phase diagram of liquid water by means of NVT and NPT MD simulations. The results confirm the existence of a density maximum at around 6 °C (279 K). Compared to popular potentials, the discrepancy between experiment and simulation for six calculated bulk properties appeared homogeneous, that is, without serious outliers. Much of the remaining work focused on the local 3D structure of liquid water, making full use of 3D snapshots and Spatial Distribution Functions (SDFs), over and above the familiar 1D radial distribution functions. The analysis of O−H...O angle distribution shows that most immediate neighbors (<2.5 Å) are hydrogen-bonded to the central molecule. Perhaps surprisingly, the impact of temperature is only minimal for molecules within 2.0 Å of the central molecule since the distribution changes only slightly at the highest temperature of 90 °C (363 K). We recover the traditional picture of a tetrahedral environment but, distinct for the QCT potential compared to others, a different shape of the SDF contour surfaces at the lone pair side of a central water. Neighboring molecules at that side form a "horseshoe"-like shape *with substantial narrowing in the central part*. In addition, "interstitial" molecules do exist but are rare. At lower temperature, well-defined secondary structures (second-shell neighbors) are observed around the central molecule. At nonambient pressures, the local environment undergoes substantial changes. A pressure increase ultimately causes the "collapse" of the second-shell molecules into the "interstitial" region, which has dramatic repercussions for the O−H...O angle distribution. The impact on the RDF is surprisingly small however. Only the OO RDF shows substantial changes, which is in good agreement with previous experimental studies. We confirm that the local hydrogen-bonding network remains largely intact even in such extreme conditions.

**Acknowledgment.** We thank Fran Painter and Simon Houlding for help with some of the NPT simulations and all NVT simulations and the EPSRC for partial funding.

**Supporting Information Available:** SDF isosurfaces generated from simulations with the QCT, SPC, and TIP5P potentials (Figure S1), radial distribution function and coordination number for a simulation generated by the QCT and TIP5P potential (Figure S2), cross-sections of the SDF with three different mutually orthogonal planes, each figure comparing three temperatures, three pressures for the QCT potential, and three potentials (Figures S3−S5), two views of the SDF of the first shell of neighboring water molecules generated by the QCT potential (Figure S6), QCT multipole moments of the atoms in water (Table S1), temperature dependence of various bulk properties obtained by NPT simulation (Table S2), and temperature dependence of constant volume heat capacity obtained by NVT simulation (Table S3). This material is available free of charge via the Internet at http://pubs.acs.org.

### References

(1) Wernet, P.; Nordlund, D.; Bergmann, U.; Cavalleri, M.; Odelius, M.; Ogasawara, H.; Naslund, L. A.; Hirsch, T. K.; Ojamae, L.; Glatzel, P.; Pettersson, L. G. M.; Nilsson, A. *Science* **2004**, *304*, 995.

(2) Smith, J. D.; Cappa, C. D.; Wilson, K. R.; Messer, B. M.; Cohen, R. C.; Saykally, R. J. *Science* **2004**, *306*, 851.

(3) Nilsson, A.; Wernet, P.; Norlund, D.; Bergmann, U.; Cavalleri, M.; Odelius, M.; Ogasawara, H.; Naslund, L.-A.; Hirsch, T. K.; Ojamae, L. *Science* **2005**, *308*, 793a.

(4) Smith, J. D.; Cappa, C. D.; Messer, B. M.; Cohen, R. C.; Saykally, R. J. *Science* **2005**, *308*, 793b.

(5) Wilson, K. R.; Cavalleri, M.; Rude, B. S.; Schaller, R. D.; Nilsson, A.; Pettersson, L. G. M.; Goldman, N.; Catalano, T.; Bozek, J. D.; Saykally, R. J. *J. Phys.: Condens. Matter* **2002**, *14*, L221.

(6) Kuo, I. F. W.; Mundy, C. J.; McGrath, M. J.; Siepmann, J. I.; VandeVondele, J.; Sprik, M.; Hutter, J.; Chen, B.; Klein, M. L.; Mohamed, F.; Krack, M.; Parrinello, M. *J. Phys. Chem. B* **2004**, *108*, 12990.

(7) Bukowski, R.; Szalewicz, K.; Groenenboom, G. C.; van der Avoird, A. *Science* **2007**, *315*, 1249.

(8) Okhulkov, A. V.; Demianets, Y. N.; Gorbaty, Y. E. *J. Chem. Phys.* **1994**, *100*, 1578.

(9) Eggert, J. H.; Weck, G.; Loubeyre, P. *J. Phys.: Condens. Matter* **2002**, *14*, 11385.

(10) Schwegler, E.; Galli, G.; Gygi, F. *Phys. Rev. Lett.* **2000**, *84*, 2429.

(11) Svishchev, I. M.; Kusalik, P. G. *J. Chem. Phys.* **1993**, *99*, 3049.

(12) Svishchev, I. M.; Zassetsky, A. Y. *J. Chem. Phys.* **2000**, *112*, 1367.

(13) Starr, F. W.; Bellissent-Funel, M. C.; Stanley, H. E. *Phys. Rev. E* **1999**, *60*, 1084.

(14) Kalinichev, A. G.; Gorbaty, Y. E.; Okhulkov, A. V. *J. Mol. Liq.* **1999**, *82*, 57.

(15) Bader, R. F. W. *Atoms in Molecules. A Quantum Theory;* Oxford Univ. Press: Oxford, GB, 1990.

(16) Popelier, P. L. A. *Atoms in Molecules. An Introduction;* Pearson: London, Great Britain, 2000.

(17) Popelier, P. L. A.; Aicken, F. M.; O'Brien, S. E. Atoms in Molecules. In *Chemical Modelling: Applications and Theory*; Royal Society of Chemistry Specialist Periodical Report; Hinchliffe, A., Ed.; 2000; Vol. 1, Chapter 3, pp 143−198.

(18) Popelier, P. L. A.; Smith, P. J. Quantum Topological Atoms. In *Chemical Modelling: Applications and Theory*; Royal Society of Chemistry Specialist Periodical Report; Hinchliffe, A., Ed.; 2002; Vol. 2, Chapter 8, pp 391−448.

(19) Popelier, P. L. A. Quantum Chemical Topology: on Bonds and Potentials. In *Structure and Bonding Intermolecular Forces and Clusters;* Wales, D. J., Ed.; Springer: Heidelberg, Germany, 2005; Vol. 115, p 1.

(20) Rafat, M.; Popelier, P. L. A. Topological atom-atom partitioning of molecular exchange energy and its multipolar convergence. In *Quantum Theory of Atoms in Molecules*; Matta, C. F., Boyd, R. J., Eds.; Wiley-VCH: Weinheim, Germany, 2007; Vol. 5, p 121.

(21) Kosov, D. S.; Popelier, P. L. A. *J. Chem. Phys.* **2000**, *113*, 3969.

(22) Kosov, D. S.; Popelier, P. L. A. *J. Phys. Chem. A* **2000**, *104*, 7339.

(23) Popelier, P. L. A.; Joubert, L.; Kosov, D. S. *J. Phys. Chem. A* **2001**, *105*, 8254.

(24) Popelier, P. L. A.; Rafat, M. *Chem. Phys. Lett.* **2003**, *376*, 148.

(25) Rafat, M.; Popelier, P. L. A. *J. Chem. Phys.* **2005**, *123*, 204103.

(26) Joubert, L.; Popelier, P. L. A. *Mol. Phys.* **2002**, *100*, 3357.

(27) Joubert, L.; Popelier, P. L. A. *Phys. Chem. Chem. Phys.* **2002**, *4*, 4353.

(28) Devereux, M.; Popelier, P. L. A. *J. Phys. Chem. A* **2007**, *111*, 1536.

(29) Handley, C. M.; Popelier, P. L. A. *Synthesis and Reactivity in Inorganic, Metal-Organic, and Nano-Metal Chemistry*; in press.

(30) Liem, S.; Popelier, P. L. A. *J. Chem. Phys.* **2003**, *119*, 4560.

(31) Liem, S.; Popelier, P. L. A.; Leslie, M. *Int. J. Quantum Chem.* **2004**, *99*, 685.

(32) Houlding, S.; Liem, S. Y.; Popelier, P. L. A. *Int. J. Quantum Chem.* **2007**, *107*, 2817.

(33) Dunning, T. H. J. *J. Chem. Phys.* **1989**, *90*, 1007.

(34) Frisch, M. J.; Trucks, G. W.; Schlegel, H. B.; Scuseria, G. E.; Robb, M. A.; Cheeseman, J. R.; Zakrzewski, V. G.; Montgomery, J. A., Jr.; Stratmann, R. E.; Burant, J. C.; Dapprich, S.; Millam, J. M.; Daniels, A. D.; Kudin, K. N.; Strain, M. C.; Farkas, O.; Tomasi, J.; Barone, V.; Cossi, M.; Cammi, R.; Mennucci, B.; Pomelli, C.; Adamo, C.; Clifford, S.; Ochterski, J.; Petersson, G. A.; Ayala, P. Y.; Cui, Q.; Morokuma, K.; Malick, D. K.; Rabuck, A. D.; Raghavachari, K.; Foresman, J. B.; Cioslowski, J.; Ortiz, J. V.; Baboul, A. G.; Stefanov, B. B.; Liu, G.; Liashenko, A.; Piskorz, P.; Komaromi, I.; Gomperts, R.; Martin, R. L.; Fox, D. J.; Keith, T.; Al-Laham, M. A.; Peng, C. Y.; Nanayakkara, A.; Gonzalez, C.; Challacombe, M.; Gill, P. M. W.; Johnson, B.; Chen, W.; Wong, M. W.; Andres, J. L.; Gonzalez, C.; Head-Gordon, M.; Replogle, E. S.; Pople, J. A. *GAUSSIAN98. Gaussian 98, Revision A.7*; Gaussian, Inc.: Pittsburgh, PA, U.S.A., 1998.

(35) Clough, S. A.; Beers, Y.; Klein, G. P.; Rothman, L. S. *J. Chem. Phys.* **1973**, *59*, 2254.

(36) Höfinger, S.; Wendland, M. *Int. J. Quantum Chem.* **2002**, *86*, 199.

(37) Maroulis, G. *Chem. Phys. Lett.* **1998**, *289*, 403.

(38) Verhoeven, J.; Dymanus, A. *J. Chem. Phys.* **1970**, *52*, 3222.

(39) Millot, C.; Soetens, J.-C.; Martins, Costa, M. T. C.; Hodges, M. P.; Stone, A. J. *J. Phys. Chem. A* **1998**, *102*, 754.

(40) Burnham, C. J.; Xantheas, S. S. *J. Chem. Phys.* **2002**, *116*, 1500.

(41) Glaettli, A.; Daura, X.; van Gunsteren, W. F. *J. Chem. Phys.* **2002**, *116*, 9811.

(42) Tironi, I. G.; Brunne, R. M.; van Gunsteren, W. F. *Chem. Phys. Lett.* **1996**, *250*, 19.

(43) Jorgensen, W. L.; Tirado-Rives, J. *Proc. Natl. Acad. Sci. U.S.A.* **2005**, *102*, 6665.

(44) Guillot, B. *J. Mol. Liq.* **2002**, *101*, 219.

(45) *MORPHY98*; a program written by P. L. A. Popelier with a contribution from R. G. A. Bone; UMIST: Manchester, England, EU, 1998.

(46) Popelier, P. L. A. *Mol. Phys.* **1996**, *87*, 1169.

(47) Gillespie, R. J.; Popelier, P. L. A. *Chemical Bonding and Molecular Geometry from Lewis to Electron Densities*; Oxford Univ. Press: New York, U.S.A., 2001.

(48) Hodges, M.; Stone, A. J.; Xantheas, S. S. *J. Phys. Chem. A* **1997**, *101*, 9163.

(49) Rafat, M.; Popelier, P. L. A. *J. Chem. Phys.* **2006**, *124*, 144102.

(50) Smith, W.; Forester, T. R. *J. Mol. Graph.* **1996**, *14*, 136.

(51) *DLPOLY*; a computer program written by W. Smith, M. Leslie, and T. R. Forester; CCLRC: Daresbury Lab, Daresbury, Warrington WA4 4AD, England, 2003.

(52) Allen, M. P.; Tildesley, D. J. *Computer Simulation of Liquids*; Clarendon: Oxford, GB, 1987.

(53) Jorgensen, W. L.; Jenson, C. *J. Comput. Chem.* **1998**, *19*, 1179.

(54) Baez, L. A.; Clancy, P. *J. Chem. Phys.* **1994**, *101*, 9837.

(55) Chaplin, M. http://www.lsbu.ac.uk/water/models.html 2007.

(56) Paesani, F.; Iuchi, S.; Voth, G. A. *J. Chem. Phys.* **2007**, *127*, 074506.

(57) Fanourgakis, G. S.; Schenter, G. K.; Xantheas, S. S. *J. Chem. Phys.* **2006**, *125*, 141102.

(58) Kell, G. S. *J. Chem. Eng. Data* **1967**, *12*, 66.

(59) Mahoney, M. W.; Jorgensen, W. L. *J. Chem. Phys.* **2000**, *112*, 8910.

(60) Yu, H.; van Gunsteren, W. F. *J. Chem. Phys.* **2004**, *121*, 9549.

(61) Finney, J. L. *Philos. Trans. R. Soc. London, Ser. B* **2004**, *359*, 1145.

(62) Svishchev, I. M.; Kusalik, P. G.; Wang, J.; Boyd, R. J. *J. Chem. Phys.* **1996**, *105*, 4742.

(63) Kusalik, P. G.; Svishchev, I. M. *Science* (*Washington, D. C.*) **1994**, *265*, 1219.

(64) Shaik, M.; Devereux, M.; Popelier, P. L. A. Submitted for publication.

(65) Woolf, L. A. *J. Chem. Soc., Faraday Trans I* **1975**, *71*, 784.

(66) Wilbur, D. J.; Defries, T.; Jonas, J. *J. Chem. Phys.* **1976**, *65*, 1783.

(67) Jonas, J.; Lee, Y. T. *J. Phys: Condens. Matter* **1992**, *4*, 305.

(68) Netz, P. A.; Starr, F. W.; Stanley, H. E.; Barbosa, M. C. *J. Chem. Phys.* **2001**, *115*, 344.

(69) Corongiu, G.; Clementi, E. *J. Chem. Phys.* **1992**, *97*, 2030.

(70) Khan, A.; Khan, M. R.; Khan, M. F.; Khanam, F. *Theochem* **2004**, *679*, 165.

(71) Urquidi, J.; Cho, C. H.; Singh, S.; Robinson, G. W. *J. Mol. Struct.* **1999**, *485*−*486*, 363.

(72) Krynicki, K.; Green, C. D.; Sawyer, D. W. *Faraday Discuss.* **1978**, *66*, 199.

(73) Weast, R. C. *Handbook of Chemistry and Physics CRC*; Boca Raton, U.S.A., 1976; Vol. 56th ed.

(74) Wagner, W.; Pruss, A. *J. Phys. Chem. Ref. Data* **2002**, *31*, 387.

CT700266N